Functional Consequences of the Kaposi's Sarcoma-Associated Herpesvirus Protease Structure: Regulation of Activity and Dimerization by Conserved Structural Elements[†,‡]

K. Kinkead Reiling,[§] Todd R. Pray,[§] Charles S. Craik,[||] and Robert M. Stroud*[,||]

Departments of Biochemistry & Biophysics and Pharmaceutical Chemistry, and Graduate Group in Biophysics, University of California in San Francisco, San Francisco, California 94143

Received May 4, 2000; Revised Manuscript Received August 15, 2000

ABSTRACT: The structure of Kaposi's sarcoma-associated herpesvirus protease (KSHV Pr), at 2.2 Å resolution, reveals the active-site geometry and defines multiple possible target sites for drug design against a human cancer-producing virus. The catalytic triad of KSHV Pr, (Ser114, His46, and His157) and transition-state stabilization site are arranged as in other structurally characterized herpesviral proteases. The distal histidine−histidine hydrogen bond is solvent accessible, unlike the situation in other classes of serine proteases. As in all herpesviral proteases, the enzyme is active only as a weakly associated dimer ($K_d \approx 2\ \mu$M), and inactive as a monomer. Therefore, both the active site and dimer interface are potential targets for antiviral drug design. The dimer interface in KSHV Pr is compared with the interface of other herpesviral proteases. Two conserved arginines (Arg209), one from each monomer, are buried within the same region of the dimer interface. We propose that this conserved arginine may provide a destabilizing element contributing to the tuned micromolar dissociation of herpesviral protease dimers.

Kaposi's sarcoma (KS)[1] has emerged as a debilitating and disfiguring disease among the human immunodeficiency virus (HIV) infected population (*5*). HIV infected men are at least 10 000 times more likely to develop aggressive KS lesions, such as peripheral effusion lymphomas (PEL) or body cavity-based lymphomas (BCBL) than the population at large (*6*). While HIV appears to be a cofactor for the development of KS, an epidemiological link relating KS to the sexual history of HIV positive patients suggested a separate transmissible etiological agent (*7*). A human herpesvirus (Kaposi's Sarcoma-associated herpesvirus, KSHV), found in PEL and BCBL neoplastic tissues, is thought to be this transmissible agent (*8*). Treatment of KS is hampered by a dearth of therapeutic agents specific for KSHV and is currently limited to compounds directed at related viruses such as herpes simplex virus (HSV) or at HIV itself (*9*).

Herpesviruses are double-stranded DNA viruses with a common viral particle architecture. They are divided into three subfamilies based on clinical characteristics, which include host cell types and natural history of infection (*10*). These subfamilies are the α-herpesviruses, which include herpes simplex virus-1 and -2 (HSV-1 and -2) and Varicella-zoster virus (VZV), the β-herpesviruses, which include human cytomegalovirus (hCMV) and human herpesviruses 6 and 7 (HHV-6, HHV-7), and the γ-herpesviruses, represented in humans by KSHV and Epstein−Barr virus (EBV). Sequence comparison of herpesviral proteases yields an average amino acid identity of 27% between subfamilies and 51% within each subfamily. Despite the clinical nature of the sub-families, similarity among the herpesviral protease structures is consistent with these classifications.

KSHV, like other herpesviruses, requires a maturational protease to generate infectious virions (*11, 12*). Formation of viral capsids is initiated by the viral assembly protein (AP), which forms a scaffold on which spherical procapsids assemble. The virally encoded serine protease KSHV Pr is expressed as an N-terminal fusion attached to roughly 10% of KSHV AP molecules (*13*). Maturation of the viral procapsid into a structure receptive to DNA packaging requires the cleavage of AP at a maturation site (M-site) near its C-terminus. In addition to processing AP at its M-site, KSHV Pr cleaves itself away from the precursor fusion protein (Pr/AP) at the release site (R-site), which separates all herpesviral protease domains from their AP constituents. The M and R sites exhibit consensus cleavage sequences of (V/L)-(N/Q/E)-A*S and Y-(V/L/I)-(K/Q)-A*S(*14*). A third proteolytic event, unique to KSHV, acts as an auto-regulatory mechanism, whereby the protease inactivates itself upon cleavage at a dimer-disruption site (D-site) (*15*). By analogy to HSV-1, inhibition of KSHV Pr will prevent maturation

[†] Research was supported by the NIH (R.M.S. and C.S.C., GM56531). K.K.R. and T.R.P. were partially supported by a graduate training Grant NIH GM08204 and by the ARCS Foundation (T.R.P.).

[‡] The coordinates have been deposited in the Brookhaven Protein Databank; accession code 1FL1.

* To whom correspondence should be addressed. Phone: (415) 476−4224. Fax: (415) 476−1902. E-mail: stroud@msg.ucsf.edu.

[§] Departments of Biochemistry & Biophysics and Pharmaceutical Chemistry.

[||] Graduate Group in Biophysics.

[1] Abbreviations: rmsd, root-mean-squared deviation; KSHV Pr, Kaposi's sarcoma-associated herpesvirus protease; KS, Kaposi's sarcoma; HIV, human immunodeficiency virus; HSV, herpes simplex virus; VZV, Varicella-zoster virus; hCMV, human cytomegalovirus; HHV-6 and HHV-7, human herpesviruses 6 and 7; EBV, Epstein−Barr virus; AP, assembly protein; NCS, noncrystallographic symmetry; CD, circular dichroism.

10.1021/bi001019h CCC: $19.00
Published on Web 09/29/2000

of virions and the subsequent dissemination of infectious viral particles (*16*−*18*).

The herpesviral protease family shares a common tertiary fold and a dependence on dimerization for proteolytic activity, despite the stability of the inactive monomer (*19*). The relatively weak micromolar dimerization affinity of herpesviral proteases (*15*, *19*−*21*) is thought to act as a regulatory mechanism that can limit protease activity to the interior of the maturing viral particle where the concentration is sufficient to support dimerization. Herpesviral proteases hydrolyze peptide bonds using a Ser-His-His catalytic triad in which the position of the aspartic acid residue seen in other classes of serine protease is occupied by a histidine. The catalytic efficiency of herpesviral proteases is lower by 100−1000-fold (in k_{cat}/K_m) relative to the trypsin family (*13*). The crystal structures of the hCMV Pr (*1*−*4*), HSV-1 and HSV-2 Pr (*22*), and VZV Pr (*23*) characterize the overall fold and allow the structural evaluation of the α- and *β*-herpesviral protease families.

We report the crystal structure of KSHV Pr at 2.2 Å resolution. This is the first structure of a *γ*-herpesviral protease to be determined. The KSHV Pr catalytic triad and oxyanion hole geometry are congruent with those of other herpesviral proteases. The hydrogen bonds, between side chains of the catalytic triad of KSHV Pr and all other herpesviral proteases, are found to be more solvent exposed than those in other classes of serine proteases. The structural divergence of the dimer interface helices among herpesviral proteases is evaluated in the context of the transition that generates the active dimer from inactive monomers. Burial of two conserved arginines (Arg234{209}),[2] one from each monomer, close to each other and within the interface of KSHV Pr is discussed in reference to the regulation of dimerization and thus activity of herpesviral proteases.

EXPERIMENTAL PROCEDURES

Protein Purification and Crystallization. KSHV Pr used for crystallization was prepared as described previously (*15*) and contained the mutation S204G, which blocks autolysis. After purification, protein was concentrated to 3.0 mg/mL using Amicon YM-10 membranes. Crystals of KSHV Pr were grown by hanging drop vapor diffusion. KSHV Pr crystallized from a mixture of 1 *μ*L of 1 mM *t*-Boc-YLKA-chloromethyl ketone (obtained from Z. Zhang and P. Ortiz de Montellano) in 10% acetonitrile, 2 *μ*L of well buffer, and 2 *μ*L of 3 mg/mL protease solution. The protease solution used in crystallization contained 25 mM potassium phosphate (pH 7.0), 10% glycerol, and 1 mM dithiothreitol. Crystallization well buffer contained 22% PEG-2K, 100 mM Tris-HCl (pH 7.5), 10% glycerol, and 190 mM $LiSO_4$. Crystals of KSHV Pr grew at 25 °C over the course of 1−2 months as small trapezoidal or hexagonal plates measuring 0.2 mm × 0.075 mm × 0.050 mm and belonging to space group $P3_121$ with unit cell dimensions $a = b = 53.58$ Å and $c = 323.06$ Å. The asymmetric unit contained a dimer, yielding a crystal solvent content of 53.7%.

[2] hCMV Pr numbering (as in refs *1*−*4*) is used, with the number in braces ({}) reflecting the residue number in the protease being addressed (e.g., KSHV Pr, VZV Pr, etc.). Nonconserved positions in sequence have both residue types listed.

Table 1: Crystallographic Statistics

data reduction resolution range (Å)	30−2.2
unique structure factors	28 220
R_{merge} (%)[a]	6.2
avg $I/\sigma(I)$	17.5
completeness (%)	99.4
mosaicity (deg)	0.40
refinement resolution range (Å)	30−2.2
no. of protein atoms	2994
no. of water molecules	195
R_{free} (%) (3σ)	26.0 (25.0)
R_{cryst} (%) (3σ)[b]	22.5 (21.5)
avg protein B (Å^2)	49.38
avg water B (Å^2)	58.35

[a] $R_{merge} = \sum|I - \langle I\rangle|/\sum|\langle I\rangle|$. [b] $R_{cryst} = \sum|F_{obs}| - |F_{calc}|/\sum|F_{obs}|$.

Data Collection, Refinement Tools. The structure was refined against a 2.2 Å data set collected at SSRL beam line 9-1 using a crystal frozen in 20% glycerol as the cryoprotectant. Diffraction data was integrated, scaled, and merged using the HKL package (*24*). The structure was solved by molecular replacement methods utilizing AMoRe (*25*) from the CCP4 suite (*26*). Noncrystallographic symmetry (NCS) averaging was performed using the program dm (*27*). Manual cycles of model rebuilding were performed using the MOLOC (*28*) graphical interface. The automated refinement of the model, including rigid body, positional, and temperature factor refinement and simulated annealing, utilized the CNS package (*29*).

Refinement Protocol. Molecular replacement was performed with a polyserine search model composed of residues 12−21, 56−109, 119−134, 154−186, and 218−256 from the structure of hCMV Pr [1CMV (*1*)]. Data from 10 Å to between 4.5 and 3.0 Å resolution yielded a postrigid body *R*-factor of 48.4% (3.0 Å). Three initial cycles of noncrystallographic symmetry (NCS) averaging of electron density maps generated using the polyserine model allowed assignment of 75% of the sequence. The model ($R_{cryst} = 37.6\%$, $R_{free} = 39.4\%$) was then subjected to multiple rounds of torsional simulated annealing, and positional and group *B*-factor minimization. NCS restraints were maintained for backbone atoms throughout refinement and for side chains until R_{free} dropped below 30%. Attention was paid throughout refinement to the possible presence of the tetrapeptide chloromethyl ketone, which was not observed in the crystal structure but was present during crystallization. Iterative rounds of manual rebuilding and automated refinement have brought the current model to crystallographic *R*-factors of 25.97% free and 22.53% cryst. The current model of KSHV Pr contains 86% (399/460 residues) of the sequence, with two loops (16−37, 117−131 in monomer A; 15−27, 121−129 in monomer B) disordered in each monomer. The model exhibits good geometry with rmsds for bond lengths and angles of 0.561 Å and 3.8°, respectively (Table 1).

Structure and Sequence Alignments and Solvent Accessibility Measurements. Structure alignments were carried out by the method of least-squares superposition as implemented in lsqman of the O suite (*30*). In all structural alignments, the *β*-barrel of the herpesviral protease structures was defined as follows: KSHV Pr *β*1 5−9, *β*2 41−43, *β*3 51−60, *β*4 65−71, *β*5 113−115, *β*6 134−137, *β*7 147−150; hCMV Pr (PDB accession codes: apo, 1CMV; inhibited, 2WPO) 14−18, 58−60, 68−77, 82−88, 131−133, 157−160, 170−173;

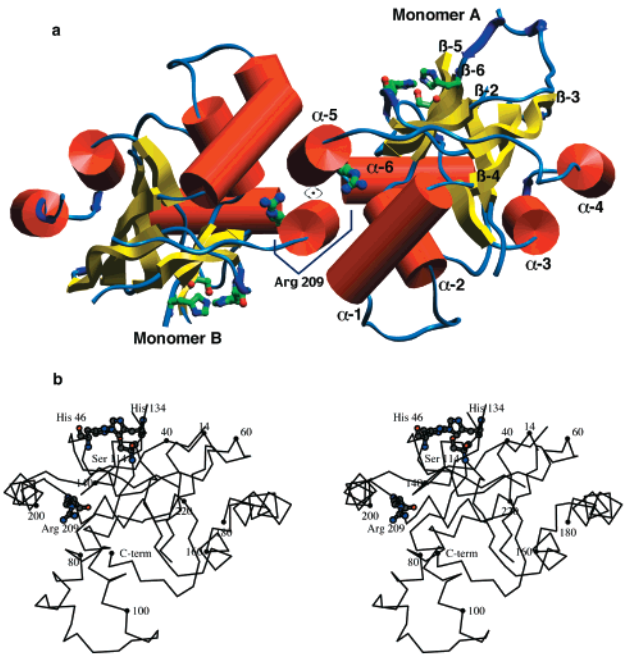

FIGURE 1: (a) Shown here is a schematic representation of the KSHV Pr dimer viewed along the dimer 2-fold axis. Secondary structure is represented with helices as cylinders in red, sheets in yellow, and loops in blue. Active-site residues His157{134}, His63-{46}, and Ser132{114} along with dimer interface Arg234{209} are rendered as ball-and-stick. (b) Monomer A is visualized as a stereo diagram with every twentieth residue numbered to indicate chain progression. As above, the active site residues and Arg234-{209} are represented as ball-and-stick.

HSV2 Pr (PDB accession code: 1AT3) 21−25, 56−58, 66−75, 80−86, 128−130, 148−151, 161−164; VZV Pr (PDB accession code: 1VZV) 13−17, 47−49, 57−66, 71−77, 119−121, 139−141, 152−155. Helices were defined as follows: KSHV Pr α1 74−84, α2 100−110, α3 154−159, α4 167−179, α5 193−203, α6 209−220; hCMV Pr 91−101, 118−128, 177−182, 190−202, 218−229, 234−245; HSV2 Pr 89−99, 115−125, 168−173, 181−193, 210−221, 226−237; VZV Pr 80−90, 106−116, 159−164, 172−184, 199−210, 215−226. Multiple sequence alignments were carried out using ClustalW (*31*). Active-site solvent accessibility was determined by the double cubic lattice method as implemented in ASC (*32*). The helical packing analysis for each protease was carried out using PROMOTIF (*33*).

RESULTS

KSHV Pr Monomer

Fold. Each monomer of KSHV Pr is composed of a seven-stranded, predominantly antiparallel β-barrel, one end of which is surrounded by a hemispherically packed set of six α-helices (Figure 1). Residues 1−87{70} form a four-stranded, twisted β-sheet, which constitutes half of the β-barrel, and the loop that presents His63{46} of the catalytic triad. Residues 90{74}−128{110} contain the first of three helical pairs (α1 and α2), which exhibit a crossing angle of 95° and pack against the end of the β-barrel proximal to the dimer interface. Loop 4 [LP4: residues 101{84}−118{100}] is in a closed conformation resulting in a 60° rotation hinged at the base of the loop or in a 12 Å shift at the end of the loop when compared to the open conformation of HSV-2

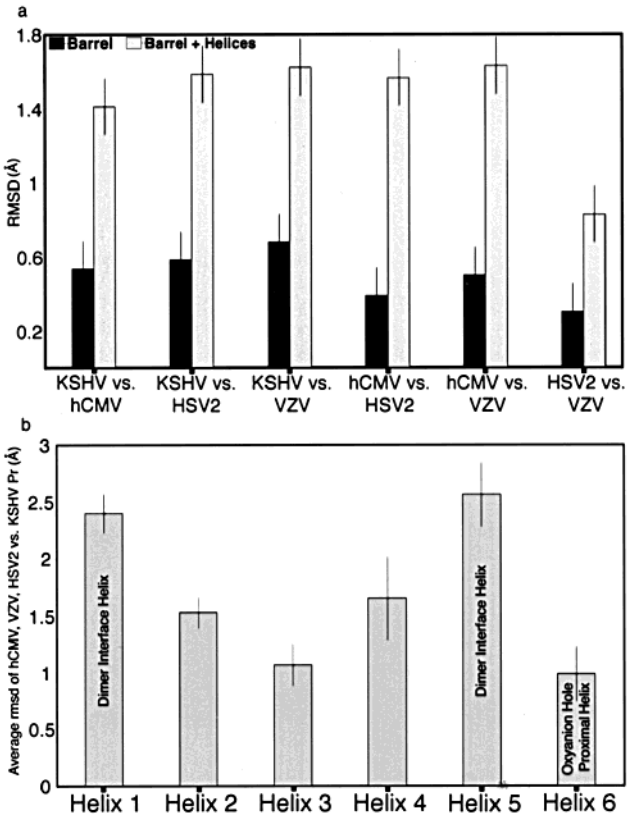

FIGURE 2: It has been suggested that the dimer interface helices may act as a structural switch in the transition from inactive monomer to active dimer (*1*, *4*). The degree of structural divergence of the dimer interface helices of herpesviral proteases suggested a conservation of mutability as a structural switch and not position. (a) The four herpesviral proteases were aligned onto the β-barrel of one monomer. RMSD values were then calculated for the β-barrel alone and the β-barrel plus the six conserved helices. (b) KSHV Pr monomer B was aligned onto the β-barrel of one monomer from hCMV, HSV2, and VZV. On the basis of this alignment, the rmsd values were calculated for each of the six-conserved α-helices. Included, as error bars, are the average error values for each helix.[3] The two most variable helices, the dimer interface helices, and the most spatially conserved helix, α6, are labeled.

Pr and VZV Pr (*23*). A second twisted sheet, formed by residues 129{111} to 175{152}, constitutes the three remaining strands of the β-barrel. Residues 176{153} to the C-terminal Ala256{230} form four helices. The first two helices (α3 and α4) pack antiparallel to each other with a crossing angle of 150°, and contact the first sheet of the β-barrel [residues 1−87{70}]. Helices α5 and α6 pack against the loops containing the central active-site His63-{46} and the oxyanion hole loop, respectively. In total, these six helices sequester 50% of the β-barrel from solvent. Helices α1 and α5 are the central features of the dimer interface, contributing 86% of the surface area buried by each monomer upon dimerization.

Structural Conservation of the Core β-Barrel with Divergence in Helical Packing. The structural similarity among herpesviral proteases is strongest within the core β-barrel, and diverges in the surrounding helices and loops (Figure 2a). The core β-barrel is conserved among the four herpesviral protease structures (KSHV, hCMV, HSV2, VZV) with an average C_α rmsd of 0.5 Å. Lesser conservation in the helical packing against the β-barrel results in an average overall C_α rmsd for the aligned secondary structures of 1.4

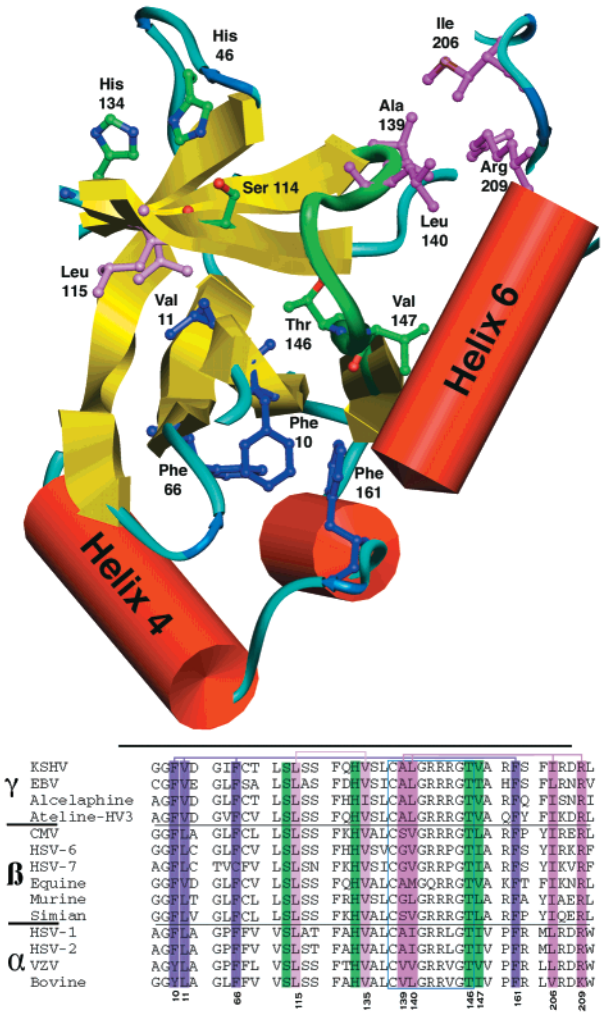

FIGURE 3: Mapping sequence conservation to the structure reveals clusters of residues conserved in both primary sequence and tertiary fold. Residues are colored identically in the multisequence alignment and in the structure of KSHV Pr. Active-site residues His157{134}, His63{46}, and Ser132{114} reside on the core β-barrel of the enzyme. Colored green in the figure and boxed in blue on the alignment, the oxyanion hole loop contains the highest concentration of conserved residues in the herpesviral protease family. Residues Leu163{140} and Ala162{139}, the N-terminal residues of the oxyanion hole loop, constitute two-thirds of a volumetrically conserved hydrophobic cluster packing against the putative dimer-destabilizing Arg234{209}. In purple, the hydrophobic bundle consisting of Phe83{66}, Phe19{10}, and Phe184{161} lies at the convergence of helices α3, α4, and α6.

Å. However, the degree of structural divergence in helical packing is not uniform and ranges from 0.88 Å rmsd for helix α6 to 2.68 Å rmsd for helix α5 (Figure 2b).

Positioned at the convergence of helices α3, α4. and α6 is a conserved aromatic bundle formed by residues Phe19{10}, Phe83{66}, and Phe184{161}. Phe19{10} and Phe83{66} emanate from β-barrel strands β1 and β4, while Phe184{161} lies within the loop connecting helices α3 and α4 (Figure 3). Structural alignment of this motif across the herpesviral proteases reveals conserved side chain packing with an average rmsd of 0.24 Å for atoms through C_β and 1.4 Å for all atoms. This conserved hydrophobic bundle may serve as an anchor point on the surface of the β-barrel stabilizing the packing of helices α3, α4, and α6. In contrast, the packing of helices α1 and α5 is predominantly defined by interactions within the dimer interface. Stabilization of helices α3, α4, and α6 by the conserved Phe-bundle as opposed to the dimerization dependent stabilization of helices α1 and α5 may contribute to the differing magnitudes of structural divergence seen in the helices of herpesviral proteases (Figure 2b).

Active Site

Environment of Catalytic Machinery and Substrate Binding Groove. KSHV Pr's catalytic triad (Ser132{114}, His63{46} and His157{134}) is located on the solvent exposed surface of strands β5 and β6 within a shallow active-site depression bracketed by helices α5 and α6 from one monomer and α1 from the other monomer. Across the active site and distal to the dimer interface, two loops (LP1 and LP0) and a helix (α0) define the extended substrate-binding site (P3, P4) in the structure of inhibited hCMV Pr(*34*). In KSHV Pr, a crystal contact near loop 1 (LP1, residues 43{34}−58{41}), helix α0 (residues 37{28}−42{33}), and loop 0 (LP0, residues 23{14}−37{28}) appears to disrupt the conformation of these structures. LP1 of KSHV Pr parallels strand β3, unlike in other herpesviral protease structures where it follows strand β6, resulting in a backbone C_α difference for KSHV Pr LP1 of up to 7 Å. In KSHV Pr, helix α0 is present as a distorted helix in one monomer, while LP0 is disordered in both. The absence of LP0 and α0 does not disturb the conformation of either the catalytic residues or the oxyanion hole, nor does it preclude the definition of the S1 binding pocket in the current KSHV Pr structure.

Catalytic Triad, S1 Binding Site, and Oxyanion Hole Are Preformed. Structural alignment of KSHV Pr with inhibited and uninhibited herpesviral proteases characterizes the catalytic triad, S1 binding pocket, and oxyanion stabilizing loop as being competent for binding and processing of substrate. KSHV Pr's catalytic triad aligns with the catalytic triads of hCMV, HSV-2, and VZV proteases with rmsds of 0.21, 1.04, and 0.73 Å (±0.15 Å).[3] By analogy to other herpesviral proteases, the backbone amide of Arg165{142}, within the oxyanion-binding loop (residues 164{141}−169{146}), forms the oxyanion-binding site of KSHV Pr (*22*, *34*) (Figure 4). This oxyanion-binding loop contains the highest concentration of conserved residues in the enzyme family (Gly164{141}, Arg165{142}, Arg166{143}, Gly168{145}, and Thr169{146}). Aligning uninhibited hCMV and VZV proteases onto the conserved β-barrel of KSHV Pr, the oxyanion loop of KSHV Pr overlays with that of the other structures with an average rmsd of 0.72 Å for main-chain atoms. This structural agreement is comparable to the 0.8 Å rmsd seen for the active-site residues in the same alignment. Thus, the conformation of the catalytic triad and oxyanion-binding site in KSHV Pr agrees with those of all other apo herpesviral protease structures.

Mapping the inhibited hCMV Pr S1 binding pocket onto KSHV Pr reveals a shallow binding groove complementary to the herpesviral consensus P1 alanine (*34*) (Figure 4). Contributors to the binding pocket include the active-site

[3] Error estimates used to report and evaluate conformational differences between groups of residues are calculated as rms. deviations between equivalent residues in monomer A to monomer B that are then averaged over all three herpesviral proteases (hCMV, HSV-2, KSHV).

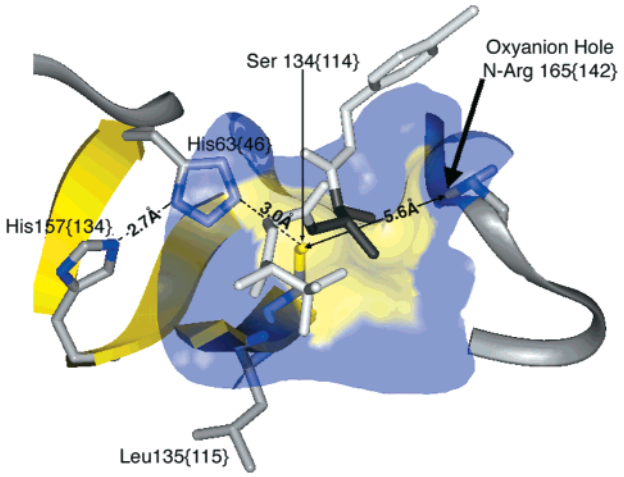

FIGURE 4: Catalytic triad and oxyanion loop are shown with a model substrate based on the inhibitor-bound hCMV Pr structure (*34*). The distances between hydrogen bonding atoms of the catalytic triad, and oxyanion hole reveal the proximity of the oxyanion loop to the catalytic residues and substrate upon binding. The model includes the P1′ to P3 residues with the P1 position darkened. A surface of the binding pocket of KSHV Pr is shown superimposed on the active site and colored yellow in regions within 3.0 Å of the modeled substrate to indicate the S1 pocket. Regions colored in blue fall between 3.0 and 4.0 Å from the substrate.

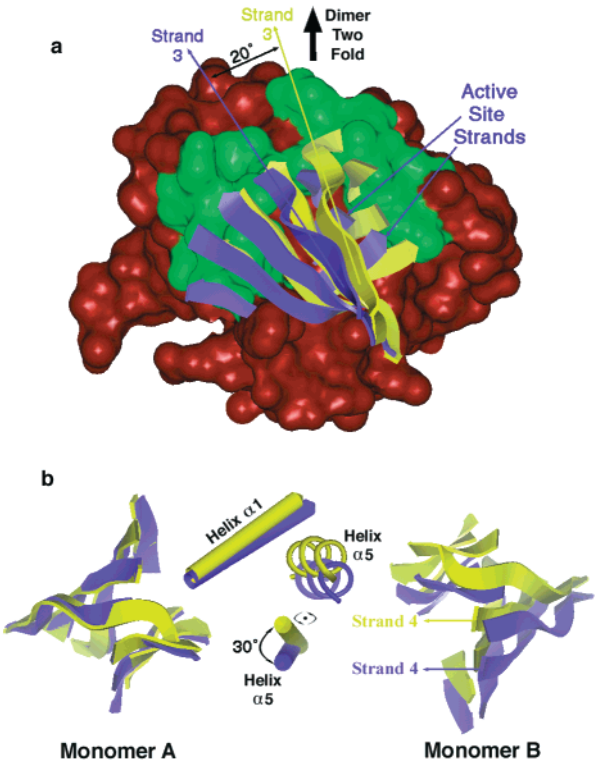

FIGURE 5: The dimer interface of KSHV Pr reveals a third mode of helical packing for a herpesviral protease further characterizing the variability in dimerization of herpesviral proteases. (a) Shown here is a view of the van der Waals surface of the KSHV Pr dimer interface in which the dimer 2-fold is oriented vertically. The surfaces of helices α1 and α5 are colored green. Pictured as ribbons in front of the surface of monomer A (mon A), the monomer B (mon B) β-barrels of KSHV Pr and hCMV Pr are represented in blue and in yellow, respectively. When the β-barrels of both KSHV Pr and hCMV Pr mon A are aligned, the position of hCMV Pr's mon B β-barrel is rotated 20° about an axis roughly perpendicular to the dimer 2-fold as compared to KSHV Pr mon B. (b) Rotated 90° about the vertical with respect to Figure 5a and now looking down the dimer 2-fold axis, Figure 5b further illustrates the 20° difference of the β-barrel of hCMV mon B and shows the 30° rotation of KSHV Pr helix α-5 within the interface.

nucleophile Ser132{114}, the oxyanion loop Arg165{142}, and the conserved Leu133{115}. On substrate binding, the carbonyl oxygen and the conserved side chain of Leu133{115} become an acceptor for the backbone amide of the substrate P1 residue and an hydrophobic contact for the P1 side chain (*34*). Leu133{115} and its neighbor, the conserved Val158{135}, adjacent in sequence to the active-site residues Ser132{114} and His157{134}, are packed against each other in the core of the β-barrel, such that alignment of the catalytic triad of all herpesviral protease structures brings these side chains into register with an average rmsd of 1.04 Å. Together, these conserved noncatalytic residues connect the positions of the substrate-binding pocket and the catalytic residues using both Val158{135} and Leu133{115} (Figure 4).

Dimer Interface

Unique Tertiary Array of Conserved Secondary Structural Elements. In contrast to the similarity in catalytic architecture among herpesviral proteases, the dimer interface of KSHV Pr differs from that of proteases of the other subfamilies. Like other herpesviral proteases, greater than 80% of the dimer interface of KSHV Pr is formed by helices α1 and α5 (Figure 1). The dimer interface α5−α5 crossing angle of 18.3° in KSHV Pr is similar to the 19.2° in hCMV, while it is different from the 50° crossing angle exhibited by the α-herpesviral proteases (VZV and HSV-2). The orientation of the β-barrels between monomers of KSHV Pr resembles that of HSV-2 and VZV, which all differ in orientation from that of hCMV by a 20° rotation about an axis roughly perpendicular to the dimer 2-fold symmetry axis. To allow for both the inter-β-barrel orientation of the α-herpesviral proteases (HSV-2 and VZV) and the α5-α5 interface helical packing of the β-herpesviral protease (hCMV), the dimer interface α5 helices in KSHV Pr are rotated 30° away from each as compared to the homologous α5 helices of hCMV Pr (Figure 5b). This 30° rotation of helix α5 distances it from helix α1, expanding and deepening the KSHV Pr dimer interface groove defined by the two helices. The dimer interface of KSHV Pr presents the conserved dimer interface secondary structural elements of this class of enzymes in a novel tertiary array and demonstrates yet a third mode of dimer interface packing for herpesviral proteases.

Disruptive Conservation. Despite the crucial role of the dimer interface as a regulator of catalysis for herpesviral proteases (*15*, *19*, *21*), sequence conservation within the interface is limited to residues Leu221{196} and Arg234{209}. The first of these, Leu221{196}, is located in the N-terminal turn of helix α5 and interacts with the catalytic triad through hydrophobic contacts to the side chain of Asp64{Leu47} in KSHV Pr, adjacent in sequence to the active site residue His63{46}. The side chains of the two conserved Arg234{209} are sequestered together, away from solvent in a hydrophobic portion of the dimer interface. The side chains are located in the groove that accepts helix α5 from the other monomer (Figure 1). Each is surrounded by two sets of clustered hydrophobic side chains from within the same monomer and residues from helices α5 and α6 of

the other monomer. Residues Ser162{Ala139}, Val163-{Leu140}, and Ile231{206} comprise the first cluster and connect this region to the base of the oxyanion loop (Figure 3). Leu238{213}, Leu235{210}, and Tyr230{Phe205} form the second cluster. The size of these clusters and the environment they create for Arg234{209} are conserved with an average side chain volume across the enzyme family for clusters one and two of 309 Å^3 (±16.51) and 388 Å^3 (±8.53), respectively. Together, these clusters orient the guanidinium groups of Arg234{209} either parallel to one another, 10 Å apart, and separated by waters as in KSHV Pr (Figure 6b) or by a cavity as in HSV-2 Pr, or to interact with each other as seen in hCMV Pr (~4 Å apart, Figure 6c) and VZV Pr (stacking). Dimerization buries two guanidinium cations within the same region of the dimer interface in all herpesviral proteases.

DISCUSSION

KSHV Pr is the first γ-herpesviral protease to be characterized at atomic resolution. Representative structures from each branch of herpesviridae now allow for a comparison between members of the three herpesviral protease subfamilies.

Active Site: Catalytic Efficiency and Active Site Solvent Accessibility. The catalytic triad H-bonding geometry of KSHV Pr and other herpesviral proteases is similar to that of other classes of serine proteases. However, the catalytic triads of herpesviral proteases are more solvent accessible than the catalytic triads of other serine proteases. This exposure may contribute to a tuned catalytic efficiency of herpesviral proteases, which is 100−1000-fold lower in k_{cat}/K_m than that seen in the trypsin family (*13*). Alignment of the catalytic residues Ser132{114}, His63{46}, and His157-{134} of KSHV Pr with the catalytic triad Ser195, His57, and Asp102 of trypsin (PDB code 1BTW) overlays the C_α of the three residues with a rmsd of 1.1 Å. The His157-{134}-N$^{\epsilon 2}$ to His63{46}-N$^{\delta 1}$ H-bond distance in KSHV Pr is 2.66 Å, close to the Asp102-O$^{\delta 2}$ to His 57-N$^{\delta 1}$ distance of 2.71 Å seen in trypsin. O$^{\delta 1}$ and O$^{\delta 2}$ of Asp102 are multiply hydrogen bonded within trypsin, and these bonds, in particular the hydrogen bond to His57-N$^{\delta 1}$, are completely shielded from solvent. This is in contrast to the hydrogen bonded atoms of His157{134}-N$^{\epsilon 2}$ and His63{46}-N$^{\delta 1}$, which retain 75% of their exposure to solvent in the context of the whole protein (Figure 7). The initial proteolytic events within the capsid are catalyzed with the protease covalently attached to the assembly protein and thus may occur in a different structural and environmental context than the isolated catalytic domains. Nevertheless, the in vivo catalytic activity of the polyprotein of HSV-1, hCMV, and SCMV (*35*) is comparable to that of the isolated protease suggesting that the catalytic parameters may be similar.

Dimer Interface: Structural Variability within a Conserved Regulator of Activity. Herpesviral proteases dimerize via helices α5 and α1 in a nonconserved fashion, as is evident from the multiple modes of helical packing seen at the dimer interface of herpesviral proteases (Figure 2). The KSHV Pr structure reveals a third dimerization mode combining topological elements from both the α- and β-herpesviral protease structures, while exhibiting a 30° rotation of helix α5 not seen in other structurally characterized herpesviral proteases. Within a single enzyme small shifts and rotations can be seen at the dimer interface, with hCMV exhibiting changes at the interface on substrate binding (6.5°) or variation in solvent conditions (*2*). Proteins structures with contact interfaces greater than 2000 Å^2 exhibit a tendency for structural reorganization upon oligomerization

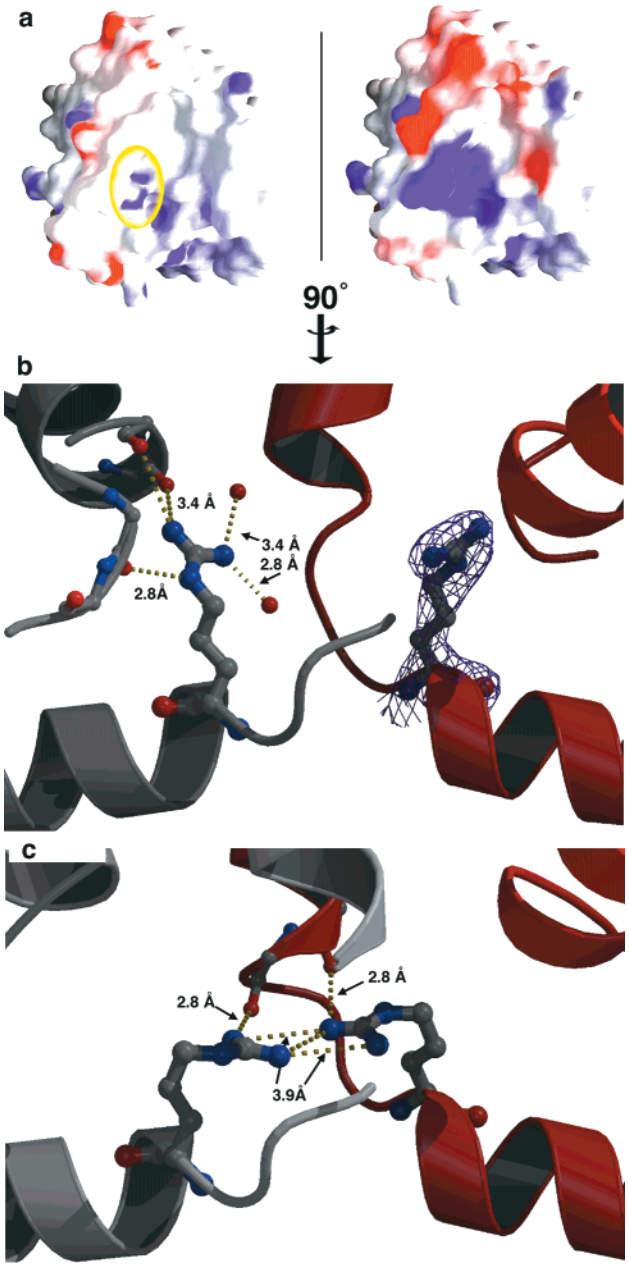

FIGURE 6: Pictured are the unfavorable electrostatic consequences of burying Arg234{209} within the ~2500 Å^2 dimer interface and the environment of Arg234{209} within the interface. (a) A GRASP (*41*) generated surface of the KSHV Pr mon A dimer interface is shown in which the electrostatic potential is calculated in the context of either the monomer (left) or the dimer (right). Positive potential is represented in blue and negative is shown in red with the two surfaces colored on a common scale. In the left image, the position of Arg234{209} in the dimer interface is highlighted. (b) Rotated 90° about the dimer 2-fold axis relative to Figure 5a, this image shows KSHV Pr Arg234{209} and its few non-hydrophobic interactions within the hydrophobic dimer interface. Electron density ($2F_o - F_c$ contoured at 1σ) is shown for Arg234{209} of one monomer. (c) Similar to the presentation in VZV, Arg234{209} of hCMV Pr interacts with its dimer 2-fold related arginine [panels b and c were produced using MOLSCRIPT (*42*)].

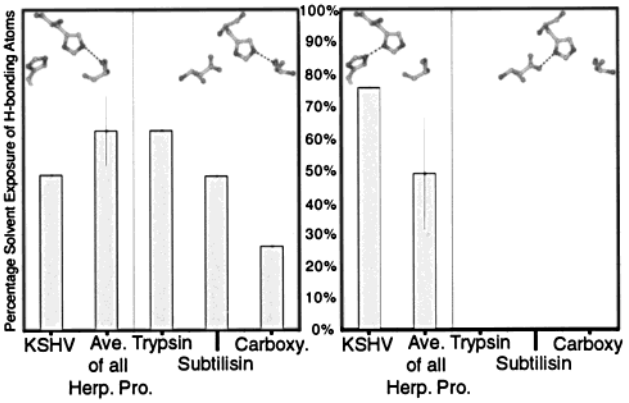

FIGURE 7: KSHV Pr and other herpesviral proteases exhibit similar percent surface area burial of the Ser-His bond, but greater percent solvent accessible surface area for the His-His bond(His-Asp in trypsin) as compared to other serine protease folds. The susceptibility of the His63{46}−His157{134} bond to the influences of bulk solvent may be a contributing factor in the reduced catalytic efficiency of herpesviral proteases (100−1000-fold as compared to mammalian trypsins). The solvent accessible surface area of the active site hydrogen bonding atoms was calculated in both the context of the entire protein and of only the catalytic triad residues. Represented here is the percentage of surface area still accessible to solvent when the catalytic triad is placed into the active site environment provided by each protease.

(*36*). The disproportionately large structural divergence of the dimer interface helices (Figure 2b) among the herpesviral proteases suggests a conservation not of position, but possibly of structural mutability. As has been previously suggested (*1*, *4*), a structural transition of helix α5 could act as a switch activating the dimeric species of herpesviral proteases.

The use of the interface helices as a route of regulation is uniquely realized in KSHV Pr through the presence of an autolytic site within helix α5. Cleavage at this D-site, between residues 228{203} and 229{204}, removes the 27 C-terminal residues, including one turn of helix α5 and all of helix α6. KSHV Pr Δ, the product of this cleavage, exhibits no detectable dimerization or activity (*15*). Circular dichroism (CD) studies on KSHV Pr Δ indicate a 47% decrease in helical content compared to dimers of full-length enzyme (*15*). While removal of residues C-terminal to the D-site would reduce helical content by only 17%, the loss of helix α6 combined with the unwinding of the dimer interface helices α1 and α5 would reduce the overall helical content by 52%, in agreement with the CD studies. Recent detection of KSHV Pr Δ in maturing capsids implicates D-site cleavage in committed in vivo self-deactivation (T.R.P., Ganem, and C.S.C., unpublished observations).

Similar spectral changes are seen during the monomer to dimer transition in full-length KSHV Pr (T.R.P. and C.S.C., manuscript in preparation) as are seen with KSHV Pr Δ. Although CD is an inexact measure of secondary structure, it communicates the degree of structural change that occurs upon D-site cleavage and during the structural transition from monomer to dimer. The most structurally conserved of the herpesviral protease helices (0.88 Å C_α rmsd, Figure 2b), helix α6 buttresses the oxyanion hole loop, burying 20% of the loop's surface. Alterations in the structure of helix α5 may affect the conformation of the loop harboring the active site His63{46}, which it contacts, or of helix α6, which it is adjacent to in sequence. Cleavage at the autolytic D-site and monomerization of full-length KSHV Pr may affect activity through the loss of crucial secondary structural elements proximal to the dimer interface (α5 and α6) and the contacts these motifs stabilize near the active site and oxyanion hole.

Dimer Interface: Burial of Two Conserved Arginines and Dimerization Affinity. Despite the burial of a hydrophobic surface area averaging 2000 Å^2 upon dimerization, herpesviral protease dimers exhibit micromolar dissociation constants. On the basis of an approximation of 20 cal of binding energy/Å^2 of hydrophobic area buried, herpesviral proteases would be expected to exhibit binding energies on the order of 40 kcal/mol, in stark contrast to the ∼10 kcal/mol seen for herpesviral proteases (*15*, *21*, *37*). Comparison of the electrostatic potential of the dimer interface of KSHV Pr in the context of both a monomer and a dimer indicates a large increase in positive potential around Arg234{209} upon dimerization (Figure 6a). The low dimerization affinity of herpesviral proteases may be due, in part, to the charge (Arg234{209}) buried by each monomers within the interface, just as substitution of an unsatisfied charge into the hydrophobic core of some proteins has been shown to be destabilizing by 2−9 kcal/mol (*38*−*40*). The energetic penalty due to reorganization of the dimer interface helices, as indicated by CD studies, combined with the cost of burying two arginine residues within the dimer interface may reduce the monomer-monomer affinity of KSHV Pr and all herpesviral proteases.

CONCLUSION

The structure of KSHV Pr, the first determined of a γ-herpesviral protease, defines the active site, the S1 substrate-binding pockets, and the dimer interface of this potential antiviral target. The herpesviral protease fold, as initially elucidated by the structures of hCMV Pr, can now be discussed in the context of a comparative analysis incorporating all three branches of herpesviridae. Sequence and structural alignments of KSHV Pr with other herpesviral proteases suggest a structural basis for the weak micromolar dimerization affinities of herpesviral proteases. Burial of a conserved arginine residue (Arg234{209}) provides a structural rationale for the weak dimerization affinity of herpesviral proteases despite their large dimer interface (2500−2700 Å^2). The observation of yet a third dimer interface conformation for a herpesviral protease, in the KSHV Pr structure, coupled with the relatively large structural divergence of the dimer interface helices supports a model in which these helices undergo an activating structural transition upon dimerization. The information distilled from the structural analysis of the three herpesviral protease subfamilies aids in understanding of the dimerization and mechanism of hydrolysis in this family of serine proteases. Structure-based development of inhibitory compounds targeted to the active site or the dimer interface may aid in the clinical treatment of KS, a common AIDS-associated neoplasm, or serve as probes useful in the study of the mechanism and regulation of herpesviral proteases.

ACKNOWLEDGMENT

We thank Richard Morse, Scott Pegg, Andrew Bogan, and Janet Finer-Moore for valuable discussions and suggestions for the manuscript. We thank Jolanta Krucinski for advice in the development of crystallization conditions. This work

is based upon research conducted at the Stanford Synchrotron Radiation Laboratory (SSRL), which is funded by the Department of Energy (BES, BER) and the National Institutes of Health (NCRR, NIGMS).

REFERENCES

1. Qiu, X., Culp, J. S., DiLella, A. G., Hellmig, B., Hoog, S. S., Janson, C. A., Smith, W. W., and Abdel-Meguid, S. S. (1996) *Nature 383*, 275−9.
2. Tong, L., Qian, C., Massariol, M. J., Bonneau, P. R., Cordingley, M. G., and Lagace, L. (1996) *Nature 383*, 272−5.
3. Shieh, H. S., Kurumbail, R. G., Stevens, A. M., Stegeman, R. A., Sturman, E. J., Pak, J. Y., Wittwer, A. J., Palmier, M. O., Wiegand, R. C., Holwerda, B. C., and Stallings, W. C. (1996) *Nature 383*, 279−82.
4. Chen, P., Tsuge, H., Almassy, R. J., Gribskov, C. L., Katoh, S., Vanderpool, D. L., Margosiak, S. A., Pinko, C., Matthews, D. A., and Kan, C. C. (1996) *Cell 86*, 835−43.
5. Ganem, D. (1997) *Cell 91*, 157−60.
6. Biggar, R. J., and Rabkin, C. S. (1996) *Hematol. Oncol. Clin. North Am. 10*, 997−1010.
7. Reitz, M. S., Jr., Nerurkar, L. S., and Gallo, R. C. (1999) *J. Natl. Cancer Inst. 91*, 1453−8.
8. Chang, Y., Cesarman, E., Pessin, M. S., Lee, F., Culpepper, J., Knowles, D. M., and Moore, P. S. (1994) *Science 266*, 1865−9.
9. Jacobson, L. P., Yamashita, T. E., Detels, R., Margolick, J. B., Chmiel, J. S., Kingsley, L. A., Melnick, S., and Munoz, A. (1999) *J. Acquired Immune Defic. Syndr. 21* (Suppl. 1), S34−S41.
10. Roizmann, B., Desrosiers, R. C., Fleckenstein, B., Lopez, C., Minson, A. C., and Studdert, M. J. (1992) *Arch. Virol. 123*, 425−49.
11. Gibson, W. (1996) *Intervirology 39*, 389−400.
12. Roizmann, B., and Sears, A. E. (1996) in *Feilds Virology* (Feilds, B. N., et al., Eds.) pp 2231−2295, Lippincott-Raven, New York.
13. Unal, A., Pray, T. R., Lagunoff, M., Pennington, M. W., Ganem, D., and Craik, C. S. (1997) *J. Virol. 71*, 7030−8.
14. Gibson, W., Welch, A. R., and Hall, M. R. T. (1994) *Perspect. Drug Discovery Des. 2*, 431−426.
15. Pray, T. R., Nomura, A. M., Pennington, M. W., and Craik, C. S. (1999) *J. Mol. Biol. 289*, 197−203.
16. Gao, M., Matusick-Kumar, L., Hurlburt, W., DiTusa, S. F., Newcomb, W. W., Brown, J. C., McCann, P. J., III, Deckman, I., and Colonno, R. J. (1994) *J. Virol. 68*, 3702−12.
17. Preston, V. G., Coates, J. A., and Rixon, F. J. (1983) *J. Virol. 45*, 1056−64.
18. Matusick-Kumar, L., McCann, P. J., 3rd, Robertson, B. J., Newcomb, W. W., Brown, J. C., and Gao, M. (1995) *J. Virol. 69*, 7113−21.
19. Darke, P. L., Cole, J. L., Waxman, L., Hall, D. L., Sardana, M. K., and Kuo, L. C. (1996) *J. Biol. Chem. 271*, 7445−9.
20. Cole, J. L. (1996) *Biochemistry 35*, 15601−10.
21. Schmidt, U., and Darke, P. L. (1997) *J. Biol. Chem. 272*, 7732−5.
22. Hoog, S. S., Smith, W. W., Qiu, X., Janson, C. A., Hellmig, B., McQueney, M. S., O'Donnell, K., O'Shannessy, D., DiLella, A. G., Debouck, C., and Abdel-Meguid, S. S. (1997) *Biochemistry 36*, 14023−9.
23. Qiu, X., Janson, C. A., Culp, J. S., Richardson, S. B., Debouck, C., Smith, W. W., and Abdel-Meguid, S. S. (1997) *Proc. Natl. Acad. Sci. U.S.A. 94*, 2874−9.
24. Otwinowski, Z., and Minor, W. (1997) in *Methods in Enzymology, Macromolecular Crystallography, part A* (Carter, C. W. J., and Sweet, R. M., Eds.) pp 307−326, Academic Press.
25. Navaza, J. (1994) *Acta Crystallogr., Sect. A 50*, 157−63.
26. Collaborative Computational Project, N. (1994) *Acta Crystallogr., Sect. D 50*, 760−63.
27. Cowtan, K. (1994) *Joint CCP4 and ESF-EACBM Newsletter on Protein Crystallography*, pp 34−8, CCP4.
28. Muller, K., Amman, H. J., Doran, D. M., Gerber, P. R., Gubernator, K., and Schrepfer, G. (1988) *Bull. Soc. Chim. Belg. 97*, 655−67.
29. Brunger, A. T., Adams, P. D., Clore, G. M., DeLano, W. L., Gros, P., Grosse-Kunstleve, R. W., Jiang, J. S., Kuszewski, J., Nilges, M., Pannu, N. S., Read, R. J., Rice, L. M., Simonson, T., and Warren, G. L. (1998) *Acta Crystallogr., Sect. D 54*, 905−21.
30. Kleywegt G. J., J. T. A. (1994) *ESF/CCP4 Newsletter 31*, 9−14.
31. Thompson, J. D., Higgins, D. G., and Gibson, T. J. (1994) *Nucleic Acids Res. 22*, 4673−80.
32. Eisenhaber, F., Lijnzaad, P., Argos, P., Sander, C., and Scharf, M. (1995) *J. Comput. Chem. 16*, 273−84.
33. Hutchinson, E. G., and Thornton, J. M. (1996) *Protein Sci 5*, 212−20.
34. Tong, L., Qian, C., Massariol, M. J., Deziel, R., Yoakim, C., and Lagace, L. (1998) *Nat. Struct. Biol. 5*, 819−26.
35. Welch, A. R., Villarreal, E. C., and Gibson, W. (1995) *J. Virol. 69*, 341−7.
36. Conte, L. L., Chothia, C., and Janin, J. (1999) *J. Mol. Biol. 285*, 2177−98.
37. Margosiak, S. A., Vanderpool, D. L., Sisson, W., Pinko, C., and Kan, C. C. (1996) *Biochemistry 35*, 5300−7.
38. Dao-pin, S., Anderson, D. E., Baase, W. A., Dahlquist, F. W., and Matthews, B. W. (1991) *Biochemistry 30*, 11521−9.
39. Stites, W. E., Gittis, A. G., Lattman, E. E., and Shortle, D. (1991) *J. Mol. Biol. 221*, 7−14.
40. Ladbury, J. E., Wynn, R., Thomson, J. A., and Sturtevant, J. M. (1995) *Biochemistry 34*, 2148−52.
41. Nicholls, A., Sharp, K. A., and Honig, B. (1991) *Proteins 11*, 281−96.
42. Kraulis, P. K. (1991) *J. Appl. Crystallogr. 24*, 946−950.

BI001019H